



**Electrode process of mobile ions in generating space-charge polarization**Atsushi Sawada  and Takaaki Manaka *Department of Electrical and Electronic Engineering, Tokyo Institute of Technology, 2-12-1, O-okayama, Meguro-ku, Tokyo 152-8552, Japan*

(Received 27 October 2023; accepted 4 February 2024; published 4 March 2024)

Macroscopic dipole moments formed in electrolytic cells influence dielectric properties of the cells, and their magnitudes can be quantified by dielectric spectroscopy. We analyze the dielectric spectra observed for dilute electrolytic cells in low-frequency regions from two perspectives: space-charge polarization and diffuse double layers on the electrodes. The difference between the two polarization phenomena is characterized by the effective dielectric constant and the kinetic parameter introduced in the Poisson-Nernst-Planck model. The analytical results indicate that the generation of space-charge polarization is attributed to the kinetic process of mobile ions replacing solvent molecules on the electrode surface. This is an experimental confirmation of the formation process of macroscopic dipole moment due to space-charge polarization and its practical contribution to the dielectric constant of material.

DOI: [10.1103/PhysRevE.109.034802](https://doi.org/10.1103/PhysRevE.109.034802)**I. INTRODUCTION**

Space-charge polarization (SCP) is a physical phenomenon in which positive and negative free charges in a material are displaced by an external electric field and form concentration gradients to generate a macroscopic electric-dipole moment in the material. The theoretical study of SCP was initiated about 70 years ago based on the Poisson-Nernst-Planck (PNP) model [1–4], and then extensive research on SCP was carried out by many researchers in the context of material science [5–12]. As SCP is often referred to as electrode polarization, dielectric spectra observed for electrolytic cells with polarizable electrodes were analyzed using the PNP model [13–18]. It was recognized in the previous studies that the PNP model describes the linear response dynamics of mobile ions perturbed from an equilibrium state, and that the capacitance of ions accumulating at the electrodes is approximately equivalent to the capacitance of diffuse double layer (DDL) derived from the Gouy-Chapman (GC) theory.

For a dilute electrolytic cell with a parallel-plate blocking electrode, DDLs can form near the electrode in equilibrium state under an external voltage application. In the GC theory, the capacitance of DDL of the dilute electrolytic cell is calculated by solving the Poisson-Boltzmann (PB) equation for a mean-field approximation level where mobile ions are considered as point charges and immersed in a continuum dielectric medium. The PNP model is also based on the same assumption that pointlike ions interact through the mean field. The standard PB model as described above can be successfully applied to systems where only Coulombic forces between pointlike ions need to be considered with respect to a mean-field level, and their electrostatic potential energies are lower than the thermal energy  $kT$ . However, it does not work well for systems with high ionic concentrations, high electrode potential, polarizable ions, and various structured ions. Therefore, properly modified PB models were developed to address each of these issues [19–24].

On the other hand, it is not well known that the standard PB model does not always reproduce the capacitances of DDL observed in very dilute electrolytic cells with nonpolar solvents. This suggests that the conventional PNP model currently in use is flawed for analyzing such cells. We have reported [25] that the capacitances of electrolytic cells, in which tetrabutylammonium cations and tetraphenylborate anions dissolved in chlorobenzene in the concentrations below  $1.0 \times 10^{-6}$  mol/L, are much larger than those predicted by the PNP model, and the underestimated values of the capacitance are attributed to the definition of dielectric constant in the PNP model. The conclusion of the study was that the dielectric effect of SCP had to be taken into account in the dielectric constant of the chlorobenzene solution in order to derive correct values of the capacitance. A further study [26] showed that the effective dielectric constant  $\epsilon_{\text{eff}}$  introduced to the PNP model is very useful for explaining experimental data, and  $\epsilon_{\text{eff}}$  depends on the polarity of solvent molecule.  $\epsilon_{\text{eff}}$  should represent the contribution of SCP and not the molecular polarization; in this sense, the root cause of its solvent polarity dependence has not been clarified yet.

Both SCP and DDL induce external charges on the electrode, but they have physically different processes. In the present work, we reconfirm the definition of SCP and discuss the difference of dielectric processes between SCP and DDL. We show that  $\epsilon_{\text{eff}}$  can represent intermediate states where the contributions of SCP and DDL are mixed in dielectric spectra. By introducing a kinetic parameter into the PNP model, we reanalyze the previously obtained experimental data of dielectric spectra and clarify the dielectric mechanism of SCP, which is related to the electrode process of mobile ions and strongly affected by the polarity of solvent molecule.

**II. DEFINITION OF SCP AND ITS CALCULATION PROCESS**

In the case that polarization density  $\mathbf{P}$  is generated in a dielectric material under an electric field  $\mathbf{E}$ , Gauss's law for

the material is expressed as  $\nabla \cdot (\varepsilon_0 \mathbf{E}) = \rho_t + \rho_p = \rho_t - \nabla \cdot \mathbf{P}$ , with  $\varepsilon_0$  the dielectric constant of vacuum,  $\rho_t$  the true charge density, and  $\rho_p$  the polarization charge density. In general,  $\mathbf{P}$  is defined in terms of bound charges confined in molecules. However, if the material contains free positive and negative charges and their distributions under the electric field induce a macroscopic dipole moment inside, the dipole-moment density should be defined as  $\mathbf{P}_{\text{SCP}}$  and included in  $\mathbf{P}$  [27]. Let  $\mathbf{P}_m$  be the molecular polarization,  $\mathbf{P} = \mathbf{P}_m + \mathbf{P}_{\text{SCP}}$ .  $\mathbf{P}_m$  produces polarization charge density  $\rho_m$ ; similarly,  $\mathbf{P}_{\text{SCP}}$  produces polarization charge density  $\rho_{\text{SCP}}$ , so  $\rho_p = \rho_m + \rho_{\text{SCP}}$ . Just as  $\mathbf{P}_m$  leads to the relative dielectric constant  $\varepsilon_m$ ,  $\mathbf{P}_{\text{SCP}}$  leads to  $\varepsilon_{\text{SCP}}$  in the same way. This argument is also justified by the concept of the multipole expansion [26]. Thus, the relative dielectric constant of the material is written as  $\varepsilon_r = \varepsilon_m + \varepsilon_{\text{SCP}}$ .

Consider a symmetric dilute electrolytic cell with a parallel-plate blocking electrode of gap  $d$ . The change in ion density under an external electric field is assumed to occur one dimensionally in the direction  $x$  perpendicular to the electrode surface. The space-charge polarization density  $P_{\text{SCP}}$  at time  $t$  is given by [10,11,28]

$$P_{\text{SCP}}(t) = ec_0(\langle x_+ \rangle - \langle x_- \rangle) = \frac{e}{d} \int_{-d/2}^{d/2} x[p(x,t) - n(x,t)]dx, \quad (1)$$

with  $e$  the elementary charge and  $c_0$  the density of positive and negative ions when no voltage is applied.  $\langle x_+ \rangle$  and  $\langle x_- \rangle$  are the mean positions of positive and negative ions in the cell, respectively.  $p(x,t)$  and  $n(x,t)$  are the densities of positive and negative ions at position  $x$  and time  $t$ , respectively, and can be calculated by using the PNP model.

Let  $J_p(x,t)$  and  $J_n(x,t)$  be the current densities of positive and negative ions, respectively, and  $E(x,t)$  be the electric field. We assume that the diffusion coefficient of positive ion is equal to that of negative ion; similarly, the mobility of positive ion is equal to that of negative ion. Thus, let  $D$  and  $\mu$  be the diffusion coefficient and the mobility for positive and negative ion, respectively. Under the conditions, the Nernst-Planck equations are expressed as

$$\begin{aligned} J_p(x,t) &= e\mu p(x,t)E(x,t) - eD\partial p(x,t)/\partial x, \\ J_n(x,t) &= e\mu n(x,t)E(x,t) + eD\partial n(x,t)/\partial x. \end{aligned} \quad (2)$$

The continuity equations are written as

$$\frac{e\partial p(x,t)}{\partial t} = -\frac{\partial J_p(x,t)}{\partial x}, \quad e\partial n(x,t)/\partial t = \partial J_n(x,t)/\partial x. \quad (3)$$

From Eqs. (2) and (3),

$$\begin{aligned} \frac{\partial p(x,t)}{\partial t} &= D\frac{\partial^2 p(x,t)}{\partial x^2} + \mu\frac{\partial}{\partial x}\left[p(x,t)\frac{\partial\Phi(x,t)}{\partial x}\right], \\ \frac{\partial n(x,t)}{\partial t} &= D\frac{\partial^2 n(x,t)}{\partial x^2} - \mu\frac{\partial}{\partial x}\left[n(x,t)\frac{\partial\Phi(x,t)}{\partial x}\right], \end{aligned} \quad (4)$$

where  $\Phi(x,t)$  is the electrical potential.

In Eq. (4), we assume that the Einstein relation  $\mu=eD/kT$  is valid.  $k$  is the Boltzmann constant and  $T$  is the absolute temperature. When the voltage applied between the electrodes is  $V(t)$ , the ion densities must satisfy the Poisson equation,

$$\partial^2 V(x,t)/\partial x^2 = -e[p(x,t) - n(x,t)]/(\varepsilon_0\varepsilon_{r0}), \quad (5)$$

where  $\varepsilon_0$  is the dielectric constant in vacuum.  $\varepsilon_{r0}$  is defined as the relative dielectric constant of solution. We also require that

$$V(t) = \int_{-d/2}^{d/2} E(x,t)dx. \quad (6)$$

We discuss the case in which a simple sinusoidal forcing voltage  $V(t)=V_1 \exp(i\omega t)$  is applied between the electrodes, where  $\omega$  is the angular frequency and  $i=\sqrt{-1}$ . The currents through the electrolytic cell,  $j_p$  and  $j_n$ , will contain all harmonics of the forcing voltage, and accurate solutions for  $p$ ,  $n$ , and  $E$  would show that they would all involve zero-frequency components with the fundamental and all its overtone. However, the ratio of higher-harmonic components to the fundamental component in  $p$ ,  $n$ , and  $E$  can be made negligible by taking  $V_1$  sufficiently small. Thus, by providing such a small  $V_1$ ,  $p$ ,  $n$ ,  $E$ ,  $j_p$ , and  $j_n$  may all be written in the form [1]

$$p(x,t) = p_0(x) + p_1(x)\exp(i\omega t), \quad (7)$$

where  $p_0$  represents the number density of positive ion in the absence of the external field. In the present case, the number density of positive ions is equal to that of negative ions in the absence of the external field, and thus we set  $p_0 = n_0 = c_0$ . Since the applied voltage contains no dc component,  $E_0 = 0$  and  $j_{p0} = j_{n0} = 0$ . If the motions of positive and negative ions under the electric field are completely blocked at the electrode surfaces and no conduction current flows across the electrodes, the boundary conditions are written as  $j_{p1}(\pm d/2) = j_{n1}(\pm d/2) = 0$ . Under the boundary condition, we obtain  $p_1(x)$  as [25]

$$p_1(x) = 2\alpha \sinh(zx), \quad (8)$$

where

$$\begin{aligned} \alpha &= \frac{V_1\mu c_0}{2d[Dz - 1/(\tau_B z)] \cosh(zd/2) + 2/(\tau_B z^2 d) \sinh(zd/2)}, \\ z &= \sqrt{(1 + i\omega\tau_B)/(D\tau_B)}, \end{aligned}$$

and  $\tau_B = \varepsilon_0\varepsilon_{r0}/(2\mu c_0 e)$ . The space-charge polarization  $P_{\text{SCP}+}$  induced by the positive ions is expressed as

$$P_{\text{SCP}+} = \frac{e}{d} \int_{-d/2}^{d/2} x p_1(x) dx. \quad (9)$$

Similarly, one obtains  $P_{\text{SCP}-}$  for the negative ions. Finally, the complex dielectric constant  $\varepsilon_{\text{SCP}}^*$  brought about by the polarization effect of positive and negative ions becomes

$$\begin{aligned} \varepsilon_{\text{SCP}}^* &= \varepsilon_{\text{SCP}}' - i\varepsilon_{\text{SCP}}'' = \frac{P_{\text{SCP}+} + P_{\text{SCP}-}}{\varepsilon_0(V_1/d)} \\ &= \varepsilon_{r0} \frac{(zd/2) - \tanh(zd/2)}{\tanh(zd/2) + i\omega\tau_B(zd/2)}, \end{aligned} \quad (10)$$

where  $\varepsilon_{r0}$  is the relative dielectric constant of solution. In the analysis of electrolyte solution using the PNP model, the relative dielectric constant of solvent,  $\varepsilon_{\text{sol}}$ , has usually been used for  $\varepsilon_{r0}$  in Eq. (10). However, if  $P_{\text{SCP}}$  is generated,  $\varepsilon_{r0}$  should be  $\varepsilon_{\text{sol}} + \varepsilon_{\text{SCP}}$  to account for  $\rho_{\text{SCP}}$ .

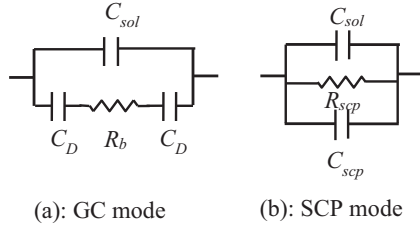


FIG. 1. Equivalent circuits representing two different polarization modes for an electrolytic cell.

### III. COMPARISON OF DIELECTRIC SPECTRA BETWEEN DIFFUSE DOUBLE LAYER AND SCP

In the present work, the difference between DDL and SCP is discussed from the perspective of the characteristics of dielectric dispersion observed in the low-frequency region for dilute electrolytic cells. The low-frequency region refers to the frequency range where the drift of mobile ions occurs under a small ac voltage application, and that is much lower than the ranges where molecular polarizations, i.e., electronic, atomic, and dipole polarizations, appear. The influence of the molecular polarizations on DDL has been extensively studied with various modified PB models proposed with different levels of mean-field approximation [19–24,29]. Here, we consider a dilute electrolytic system to which the standard PB model, assuming pointlike ions, is applicable. DDL is characterized by the behavior of mobile ions being attracted to the counter charges of electrode, and the external electric field is screened by the mobile ions accumulated near the electrode. On the other hand, SCP generates a macroscopic dipole moment in the bulk under the influence of electrode charges, and its function of compensating the electrode charges in terms of dielectricity is similar to that of the molecular molarization. The electric-field screening and the electrode charge compensation are physically different phenomena.

As shown in Fig. 1(a), a DDL near the electrode is represented by a capacitor  $C_D$ , the thickness of which is equal to the Debye length, and the bulk layer between the two capacitors is represented by a resistor  $R_b$ . (GC mode) It is assumed that there is no specific adsorption of ions on the electrodes and the distance between the electrodes is sufficiently large compared to the Debye length. For the SCP mode the space between the electrodes is filled with a dielectric material with the relative dielectric constant  $\epsilon_{\text{sol}} + \epsilon'_{\text{SCP}}$  and dielectric loss  $\epsilon''_{\text{SCP}}$ , resulting in a parallel connection with capacitors  $C_{\text{sol}}$  and  $C_{\text{SCP}}$  and a resistor  $R_{\text{SCP}}$ . Here,  $C_{\text{sol}}$  represents a solvent capacitance. The difference between the GC and SCP modes is that for a potential difference externally given to the cell, potential drop occurs in the diffuse layers in the GC mode, while it occurs throughout the material between the electrodes in the SCP mode [30].

Converting the series circuit consisting of two  $C_D$ s and  $R_b$ , excluding  $C_{\text{sol}}$  in GC mode in Fig. 1(a), into an equivalent parallel circuit yields the equivalent parallel capacitance  $C_p = 2C_D / (4 + \omega^2 R_b^2 C_D^2)$  per unit area and the equivalent parallel resistance  $R_p = R_b + 4 / (\omega^2 R_b C_D^2)$ . Here,  $C_D = \epsilon_0 \epsilon_{\text{sol}} / L_D$ , where  $L_D$  is the Debye length expressed as  $L_D = \sqrt{\epsilon_0 \epsilon_{\text{sol}} kT / (2e^2 c_0)}$ , and  $R_b = d / (2c_0 \mu e)$ . Replacing  $\epsilon_r$

in  $\tau_B$  by  $\epsilon_{\text{sol}}$ , i.e.,  $\tau_B = \epsilon_0 \epsilon_{\text{sol}} / (2\mu c_0 e)$ , the complex dielectric constant of the GC mode,  $\epsilon_{\text{GC}}^*$ , is expressed as  $\epsilon_{\text{GC}}^* = \epsilon'_{\text{GC}} - i\epsilon''_{\text{GC}}$ , where

$$\epsilon_{\text{GC}}' = \frac{dC_p}{\epsilon_0} = \frac{\epsilon_{\text{sol}}(\tau_0/\tau_B)}{1 + \omega^2 \tau_0^2}, \quad (11)$$

$$\epsilon_{\text{GC}}'' = \frac{d}{\omega \epsilon_0 R_p} = \frac{\epsilon_{\text{sol}} \omega (\tau_0^2/\tau_B)}{1 + \omega^2 \tau_0^2}, \quad (12)$$

and  $\tau_0 = (d/2)\sqrt{\tau_B/D}$ . It is found from the forms of the equations that  $\epsilon_{\text{GC}}^*$  exhibits a Debye-type dielectric relaxation. The  $\epsilon_{\text{SCP}}^*$  of the SCP mode is expressed as Eq. (10). Replacing  $\epsilon_{r0}$  by  $\epsilon_{\text{sol}}$  in Eq. (10) and applying the approximations  $\tanh(zd/2) \approx 1$ ,  $z \approx 1/\sqrt{D\tau_B}$ ,  $d/(2\sqrt{D\tau_B}) \gg 1$ ,  $\epsilon'_{\text{SCP}}$  and  $\epsilon''_{\text{SCP}}$  in Eq. (10) have exactly the same form as Eqs. (11) and (12), respectively.

It has been shown in Ref. [26] that the GC mode and the SCP mode can be quantitatively identified in terms of the magnitude of  $\epsilon_{\text{eff}}$ . Here, the maximum value of  $\epsilon_{\text{SCP}}$  must be known because the value of  $\epsilon_{\text{eff}}$  cannot exceed the value of  $\epsilon_{\text{sol}} + \epsilon_{\text{SCP}}$ . The maximum value  $\epsilon_{\text{SCP}(\text{max})}$  is calculated from the low-frequency limit of the real part in Eq. (10) and it becomes  $d^2 e^2 c_0 / (8\epsilon_0 kT)$ . Thus,  $\epsilon_{\text{eff}}$  takes values between  $\epsilon_{\text{sol}}$  and  $\epsilon_{\text{sol}} + \epsilon_{\text{SCP}(\text{max})}$ . Defining  $\epsilon_{\text{max}}$  as the maximum value of  $\epsilon_{\text{eff}}$ , then  $\epsilon_{\text{max}} = \epsilon_{\text{sol}} + \epsilon_{\text{SCP}(\text{max})}$ . Assuming that  $c_0 = 1.0 \times 10^{20} \text{ m}^{-3}$ ,  $d = 2.26 \times 10^5 \text{ m}$ , and  $T = 293 \text{ K}$ ,  $\epsilon_{\text{SCP}(\text{max})}$  is calculated to be 4565. When  $\epsilon_{\text{sol}} = 5.0$ , the value of  $\epsilon_{\text{max}}$  is 4570. By using Eq. (10) with  $D = 7.0 \times 10^{-10} \text{ m}^2/\text{s}$ , the simulated frequency dependences of  $\epsilon_{\text{SCP}}^*$  for four  $\epsilon_{\text{eff}}$  values, including the intermediate values 45.7 ( $= \epsilon_{\text{max}}/100$ ) and 457 ( $= \epsilon_{\text{max}}/10$ ), are shown in Fig. 2 as solid lines. The open circles in the figures show the frequency-dependent behaviors of  $\epsilon'_{\text{GC}}$  and  $\epsilon''_{\text{GC}}$  calculated using Eqs. (11) and (12), respectively, with  $\epsilon_{\text{sol}} = 5.0$ .

It is found from Fig. 2 that as  $\epsilon_{\text{eff}}$  increases, the relaxation frequency shifts to lower frequencies and the low-frequency plateau value of  $\epsilon'_{\text{SCP}}$  increases. A significant difference between  $\epsilon'_{\text{SCP}}$  and  $\epsilon'_{\text{GC}}$  for  $\epsilon_{\text{eff}} = \epsilon_{\text{sol}} = 5.0$  appears in the high-frequency region.  $\epsilon'_{\text{GC}}$  decreases with frequency with a slope of  $-2$ ; however, the slope of  $\epsilon'_{\text{SCP}}$  changes from  $-2$  to  $-1.5$  in the range between 1000 and 10 000 Hz. The  $f^{-1.5}$  dependence of  $\epsilon'_{\text{SCP}}$  in the high frequencies is often invisible in actual measurements, because it is hidden by the contribution of molecular polarization to  $\epsilon'_r$ . Therefore, it has been believed for a long time that  $\epsilon'_{\text{SCP}}$  exhibits  $f^{-2}$  dependence [3,15,17,31–33]. The difference between  $\epsilon'_{\text{SCP}}$  and  $\epsilon'_{\text{GC}}$  mainly comes from the assumption that  $z \approx 1/\sqrt{D\tau_B}$  providing  $\omega\tau_B \rightarrow 0$ . The assumption is valid for small values of  $\epsilon_{\text{sol}}$  included in  $\tau_B$ ; however, it collapses when the contribution of  $\epsilon_{\text{SCP}}$  becomes significantly large. As shown in Fig. 2(a), the frequency at which the slope of  $\epsilon'_{\text{SCP}}$  changes from  $-2$  to  $-1.5$  shifts to the lower-frequency side as  $\epsilon_{\text{eff}}$  increases. Thus, the frequency dispersion of  $\epsilon'_{\text{SCP}}$  is inherently  $f^{-1.5}$  dependent. Experimentally, obvious  $f^{-1.5}$  dependences of  $\epsilon'_r$  have been observed not only for very dilute electrolytic solutions [30,34] but also for liquid crystals [35–41] and polymers [42] containing impurity ions. A common point for these experimental results is that the ion concentrations in the materials are quite low and the polarities of the matrix materials are comparably low.

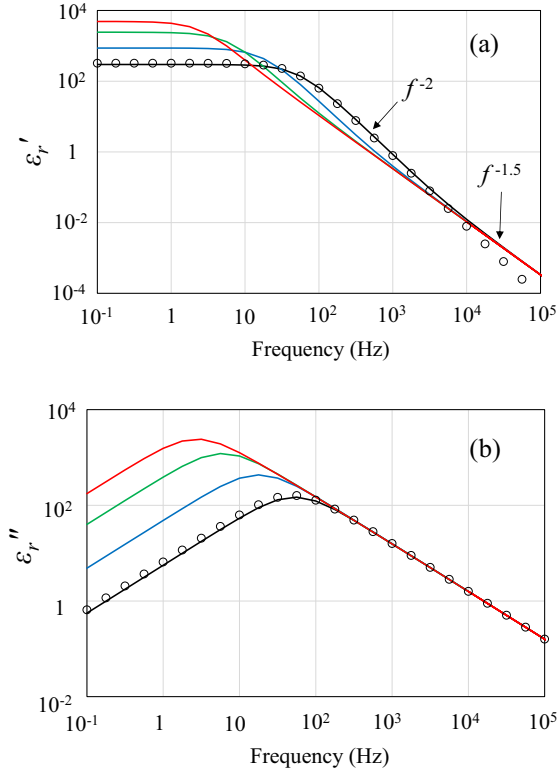


FIG. 2. Frequency dependences of complex dielectric constant with  $\epsilon_{\text{eff}}$  as a parameter. (a) Relative dielectric constant. (b) Relative dielectric loss factor. Black lines:  $\epsilon_{\text{SCP}}^*$  with  $\epsilon_{\text{eff}} = 5$ ; blue lines:  $\epsilon_{\text{SCP}}^*$  with  $\epsilon_{\text{eff}} = 45.7$ ; green lines:  $\epsilon_{\text{SCP}}^*$  with  $\epsilon_{\text{eff}} = 457$ ; red lines:  $\epsilon_{\text{SCP}}^*$  with  $\epsilon_{\text{eff}} = 4570$ ; and open circles:  $\epsilon_{\text{GC}}^*$  with  $\epsilon_{\text{sol}} = 5$ .

#### IV. KINETIC PROCESS OF MOBILE IONS ON ELECTRODES

We have used tetrabutylammonium tetraphenylborate (TBATPB) for experiments as an electrolyte and added it to several solvents at different concentrations. TBA<sup>+</sup> and TPB<sup>-</sup> ions are known to be difficult to form solvated ions in various organic solvents and their Stokes radii are nearly the same, which are about 4 Å [43,44]. It has been found in Ref. [26] that TBA<sup>+</sup> and TPB<sup>-</sup> dissolved in chlorobenzene (CB) completely follows the SCP mode, while those in 1,2-dichlorobenzene (o-DCB) or dimethyl sulfoxide (DMSO) behave as a GC-SCP mixed mode. The origin of such a solvent dependence can be attributed to the behaviors of TBA<sup>+</sup> and TPB<sup>-</sup> as they approach the electrode surface. To reach the electrode under an external electric field, the ions must push away and replace solvent molecules attached to the electrode. This situation is schematically illustrated in Fig. 3.

As shown in the inset of Fig. 3, electrons are expelled from the electrode surface by quantum mechanical effects, leaving a positively charged layer behind [45–47]. Thus, an electric double layer is formed. Under the influence of the electric field created by the electric double layer, solvent molecules in contact with the electrode surface are polarized [48,49]. According to the first-principles calculation results on the structure of metal–liquid interface [50,51], the dipoles of liquid molecules in contact with a metal prefer to be oriented

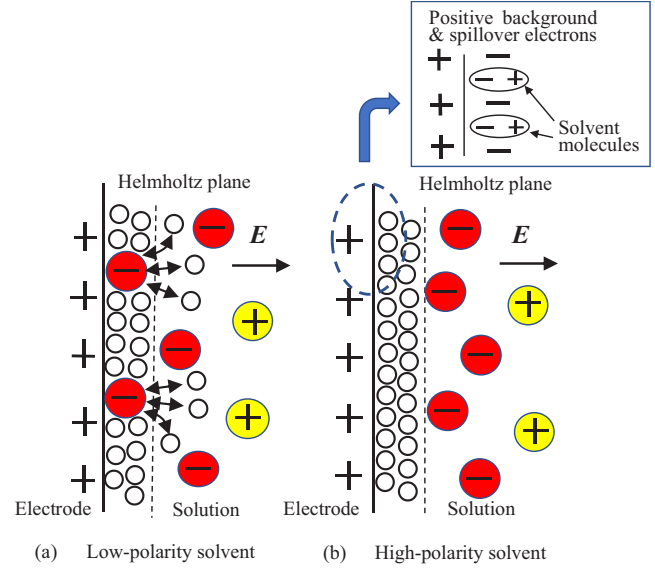


FIG. 3. Replacement of solvent molecules by ions at an electrode surface. Yellow cations and red anions represent TBA<sup>+</sup> and TPB<sup>-</sup>, respectively. Open circles are solvent molecules. Inset shows an electric double layer due to the electronic spillover at the electrode surface and induced polarizations of solvent molecules.

perpendicular to the surface, which increases attractive force at the interface. Since the values of electric dipole moment  $\mu_d$  for CB, o-DCB, and DMSO are 1.55, 2.25, and 3.96D, respectively, the magnitude of the attractive force to the electrode should be in the order of CB < o-DCB < DMSO. The calculation results of image forces given in Appendix A also suggest that it may be easy for a TBA<sup>+</sup> or TPB<sup>-</sup> ion to replace CB molecules, but more difficult to replace o-DCB molecules, and even more difficult to replace DMSO molecules.

Here, we introduce a rate constant  $\xi_a$ , which represents the rate to replace solvent molecules by ions, into the boundary condition of the PNP model. The same value of  $\xi_a$  is assumed for both TBA<sup>+</sup> and TPB<sup>-</sup>. The mathematical process of  $\xi_a$  as the boundary condition is the same as that of the rate constant  $\xi$ , which was introduced by Chang and Jaffe [2] and represents the discharge rate of ions at electrodes. The physical interpretation of  $\xi_a$  is, however, different from that of  $\xi$ . When  $\xi_a = 0$ , the drifts of TBA<sup>+</sup> and TPB<sup>-</sup> under an external field are completely blocked at the Helmholtz plane in Fig. 3. When  $\xi_a > 0$ , some amount of TBA<sup>+</sup> and TPB<sup>-</sup> enter the Helmholtz layers and replace solvent molecules depending on the magnitude of  $\xi_a$ . The fact that TBA<sup>+</sup> and TPB<sup>-</sup> reach the electrodes results in generating  $P_{\text{SCP}}$  in bulk and inducing  $\rho_{\text{SCP}}$  at interfaces, which compensates true charges on the electrodes.

The PNP equation is solved considering  $\xi_a$  to the boundary condition. The other calculation conditions are the same as those for Eq. (10). The rate to replace solvent molecules is proportional to the difference between instantaneous values of ion concentration at the electrodes, i.e.,  $p(-d/2)$ ,  $n(-d/2)$  or  $p(d/2)$ ,  $n(d/2)$ , and the undisturbed concentration  $p_0 = n_0 =$



$c_0$ . Thus, the pertinent boundary condition is expressed as

$$\begin{aligned} j_{p1}\left(\pm\frac{d}{2}\right) &= \pm\xi_a e p_1\left(\pm\frac{d}{2}\right), \\ j_{n1}\left(\pm\frac{d}{2}\right) &= \mp\xi_a e n_1\left(\pm\frac{d}{2}\right). \end{aligned} \quad (13)$$

Under the conditions of Eq. (13), the solution for  $p_1(x)$  is expressed as

$$p_1(x) = \frac{\mu c_0 V_1 \tanh(zx)}{d\left\{\left[\frac{2}{dz^2\tau_B} + \xi_a\right] \tanh(zx) - \frac{1}{z\tau_B} + Dz\right\}}. \quad (14)$$

The current density  $j_1 (= j_{p1} + j_{n1})$  becomes

$$j_1 = \varepsilon_0 \varepsilon_{\text{sol}} \frac{dE(t)}{dt} + e \left[ 2\mu c_0 E_1 - D \frac{dp_1}{dx} + D \frac{dn_1}{dx} \right], \quad (15)$$

where  $\varepsilon_{\text{sol}}$  is the relative dielectric constant of solvent. The total current density  $J_1$  flowing into the electrolyte layer can be obtained by taking a space average of  $j_1$  over the whole layer, and we obtain

$$\begin{aligned} J_1 &= i\omega\varepsilon_0\varepsilon_{\text{sol}} \frac{V_1}{d} + \frac{e}{d} \left\{ 2\mu c_0 V_1 - D \left[ p_1\left(\frac{d}{2}\right) - p_1\left(-\frac{d}{2}\right) \right] \right. \\ &\quad \left. + D \left[ n_1\left(\frac{d}{2}\right) - n_1\left(-\frac{d}{2}\right) \right] \right\}. \end{aligned} \quad (16)$$

The admittance per unit area,  $Y_1 (= J_1/V_1)$ , is expressed as

$$\begin{aligned} Y_1 &= \frac{i\omega\varepsilon_0\varepsilon_{\text{sol}}}{d} + \frac{2e\mu c_0}{d} \\ &\quad - \frac{4e\mu c_0 D}{d^2} \frac{\tanh\left(\frac{zd}{2}\right)}{\left[\frac{2}{dz^2\tau_B} + \xi_a\right] \tanh\left(\frac{zd}{2}\right) - \frac{1}{z\tau_B} + Dz}. \end{aligned} \quad (17)$$

The parallel resistance per unit area  $R_B(\omega)$  and the parallel capacitance per unit area  $C_B(\omega)$  given by the sum of the space-charge capacitance and the geometrical capacitance are written as  $R_B(\omega) = 1/Y'_1$  and  $C_B(\omega) = Y''_1/\omega$ , respectively, providing that  $Y_1 = Y'_1 + iY''_1$ . Thus, we obtain the complex dielectric constant  $\varepsilon_B^*$  as

$$\varepsilon_B^* = \varepsilon_B' - i\varepsilon_B'', \quad (18)$$

where

$$\varepsilon_B' = \frac{dC_B}{\varepsilon_0} = \frac{dY_1''}{\omega\varepsilon_0}, \quad (19)$$

$$\varepsilon_B'' = \frac{d}{\omega\varepsilon_0 R_B} = \frac{dY_1'}{\omega\varepsilon_0}. \quad (20)$$

The first term on the right side of Eq. (17) represents the solvent capacitance. By excluding the first term and setting  $\xi_a = 0$ , Eq. (18) agrees with  $\varepsilon_{\text{SCP}}^*$  using Eq. (10).

In the present work, the equivalent circuit shown in Fig. 4 is used for data analysis.  $C_m$  is the capacitance representing the dipole layer on electrode surface;  $R_m$  is the resistance representing the leak current through the dipole layer.  $C_B(\omega)$

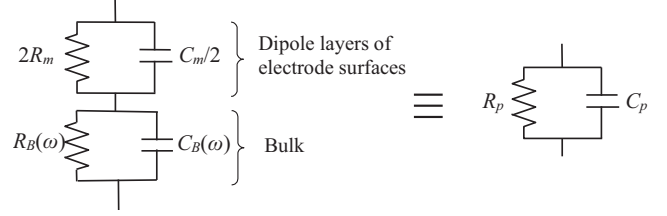


FIG. 4. Equivalent circuit of an electrolytic solution cell.

and  $R_B(\omega)$  are the capacitance and resistance calculated with Eqs. (19) and (20), respectively.  $C_p$  and  $R_p$  are the parallel capacitance and resistance per unit area, which are used for data acquisition of  $\varepsilon_r^* = \varepsilon_r' - i\varepsilon_r''$  in measurements, where  $\varepsilon_r' = dC_p/\varepsilon_0$  and  $\varepsilon_r'' = d/(\omega\varepsilon_0 R_p)$ . The changes in the frequency dependence of  $\varepsilon_r^*$  are simulated with different values of  $\xi_a$  and the results are shown in Fig. 5. The physical parameters used for the calculation are  $D = 7.0 \times 10^{-10} \text{ m}^2/\text{s}$ ,  $c_0 = 1.0 \times 10^{20} \text{ m}^{-3}$ ,  $\varepsilon_{\text{sol}} = 5$ ,  $\varepsilon_{\text{eff}} = 4570$ ,  $C_m = 0.1 \text{ F/m}^2$ ,  $R_m = 1.0 \times 10^4 \text{ }\Omega/\text{m}^2$ ,  $T = 293 \text{ K}$ , and  $d = 2.26 \times 10^{-5} \text{ m}$ . The relaxation frequency of  $\varepsilon_r^*$  in the low-frequency region shifts to higher frequencies with increasing  $\xi_a$ . The influence of  $\xi_a$  on  $\varepsilon_r'$  in the high-frequency region, where the contribution of  $P_{\text{SCP}}$  is dominant, becomes visible with the values of  $\xi_a$  larger than  $1.0 \times 10^{-5} \text{ m/s}$  [52].

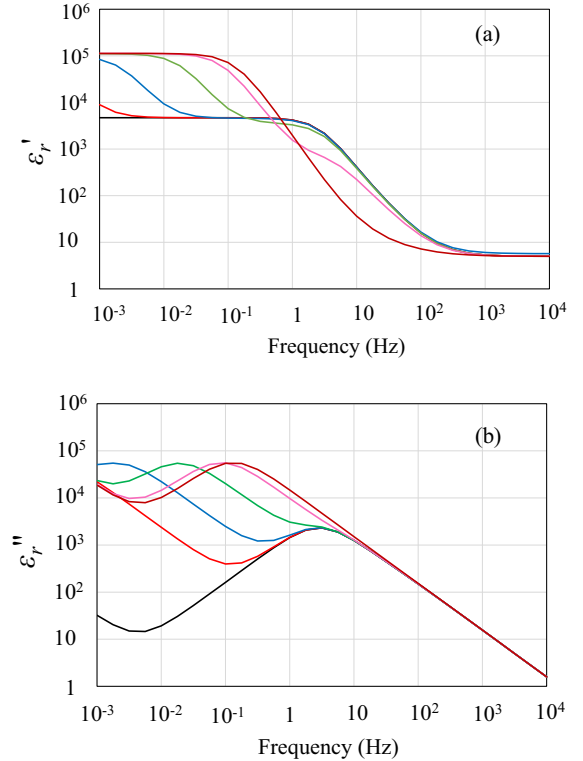


FIG. 5. Frequency dependence of  $\varepsilon_r^*$  with  $\xi_a$  as a parameter. (a) Relative dielectric constant. (b) Relative dielectric loss factor. Black lines:  $\xi_a = 0 \text{ m/s}$ ; red lines:  $\xi_a = 10^{-7} \text{ m/s}$ ; blue lines:  $\xi_a = 10^{-6} \text{ m/s}$ ; green lines:  $\xi_a = 10^{-5} \text{ m/s}$ ; pink lines:  $\xi_a = 10^{-4} \text{ m/s}$ ; and brown lines:  $\xi_a = 10^{-3} \text{ m/s}$ .

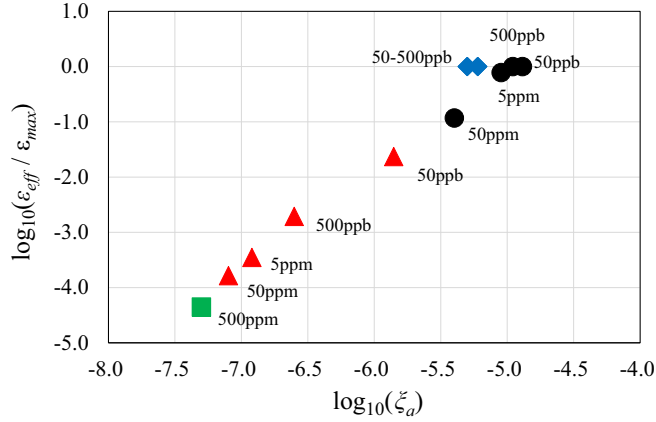


FIG. 6. Correlation between  $\xi_a$  and  $\epsilon_{\text{eff}}/\epsilon_{\text{max}}$ . Each symbol represents different solvent:  $\blacklozenge$  BB,  $\bullet$  CB,  $\blacktriangle$  o-DCB, and  $\blacksquare$  DMSO. The numbers next to symbols represent the concentrations of TBATPB in solution samples given in Table II.

## V. DATA ANALYSIS AND DISCUSSION

We use reported data of complex dielectric constant given in Ref. [26] for the present analysis. The data were obtained for TBATPB solutions with different solvent, CB, o-DCB, or DMSO. Data for another solvent, bromobenzene (BB), were added to the present analysis. The solution sample preparation and measurement condition are summarized in Appendix B. We analyzed the dielectric spectra observed for the solution samples and determined physical parameters by a curve-fitting process with calculated values. The examples of the dielectric spectra and the values of physical parameters are shown in Appendix C.

The unit of  $\xi_a$  is m/s, which represents velocity. If the effective value of the voltage applied to the cell is  $V_{\text{app}}$  and the average electric field in the cell is  $E_{\text{av}}$ , then  $E_{\text{av}} = V_{\text{app}}/d = 221$  V/m in the present condition. The drift velocity  $v_{\text{av}}$  of ions under an average electric field through the cell is calculated to be  $v_{\text{av}} = \mu E_{\text{av}}$ . Comparing the values of  $v_{\text{av}}$  with those of  $\xi_a$  given in Table IV in Appendix C, we find that  $v_{\text{av}} < \xi_a$  and  $\epsilon_{\text{eff}}/\epsilon_{\text{max}} = 1$  for all the solutions of BB and the 50 ppb-5 ppm solutions of CB, while  $v_{\text{av}} > \xi_a$  and  $\epsilon_{\text{eff}}/\epsilon_{\text{max}} < 1$  for all the solutions of o-DCB and the 500 ppb solution of DMSO. Figure 6 shows the logarithms plot of  $\xi_a$  and  $\epsilon_{\text{eff}}/\epsilon_{\text{max}}$  values where  $\blacklozenge$  BB solution,  $\bullet$  CB solution,  $\blacktriangle$  o-DCB solution,  $\blacksquare$  DMSO solution, and a strong correlation between them was observed. The numbers in the graph indicate the concentrations of TBATPB in solution samples given in Table II. The ratio of  $v_{\text{av}}$  to  $\xi_a$  is regarded as the ratio of the bulk current density  $J_b$  to the Helmholtz layer current density  $J_H$ . From this point of view, the behaviors of TBA<sup>+</sup> and TPB<sup>-</sup> ions in BB and CB are considered to be operating in the SCP mode because the impedance of the Helmholtz layer is lower than that of bulk layer, while those in o-DCB and DMSO are operating in the GC-SCP mixed mode because the impedance of the Helmholtz layer is higher. As expected, if  $J_b \gg J_H$ , the polarization process of mobile ions in the cell approaches the GC mode.

In our previous work [26], we analyzed experimental data by introducing a different boundary condition into the PNP

model, which represented the adsorption-desorption process of mobile ions on electrodes. The measured values of  $\epsilon_r^*$  for the solution samples shown in Table II were well fitted by the calculated values in the previous analysis as well as in the present analysis. We then revisited the previous result and found that for CB solutions with low concentrations of TBATPB, there was a discrepancy in which the number of adsorbed ions exceeded the total number of ions in the cell in a single measurement. Accordingly, the experimental results could not be explained by the adsorption-desorption model. In fact, the measured values of  $\epsilon_r^*$  were reproducible in repeated measurements within a short period of about one hour, suggesting invalidity of the adsorption-desorption model.

## VI. CONCLUSION

We have found that the dielectric spectra brought about by the SCP differ significantly from those by the DDL and they can be characterized by the magnitude of  $\epsilon_{\text{eff}}$  introduced in the PNP model and the values of  $\xi_a$  determined in analyzing the dielectric spectra of the electrolytic solutions are clearly correlated with  $\epsilon_{\text{eff}}/\epsilon_{\text{max}}$ . This result indicates that the generation of SCP in the electrolytic cells originates from the kinetic process of mobile ions to replace solvent molecules at the electrode surfaces. This is an experimental confirmation of  $P_{\text{SCP}}$  and its practical contribution to the dielectric constant of material. A deep understanding of  $P_{\text{SCP}}$  will not only improve analytical techniques using dielectric spectroscopy, but also provide a perspective for the development of dielectric materials.

## APPENDIX A: IMAGE FORCES OF CHARGE AND DIPOLE

The image-charge method is very useful for calculating the electric field generated by a point charge  $+q$  placed near a conductor plate. As shown in Fig. 7(a), by treating the conductor as a mirror, an image charge is assumed at a point symmetrically opposite of  $+q$ . Since the true charge  $+q$  feels a force from the conductor owing to the electric field, the force  $F_c$  can be calculated. It is expressed as

$$F_c = \frac{q^2}{4\pi\epsilon_0(2a)^2} = \frac{q^2}{16\pi\epsilon_0 a^2}, \quad (\text{A1})$$

where  $a$  is the distance between the conductor surface and the point charge. Since the image charge is opposite in sign of a true charge,  $F_c$  is always attractive force.

The same concept can be used to calculate the attractive force  $F_d$  when the electric dipole is placed near the conduc-

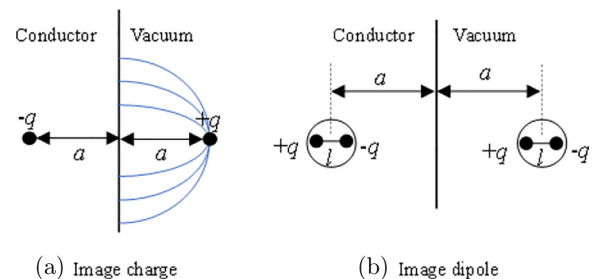


FIG. 7. Method of image charges.

TABLE I. Comparison of image forces between ion and solvents.

Molecule	Radius $r$ (m)	Electric dipole moment		Image force				
		$\mu_d$ (debye)	$\mu_d$ (Cm)	$F_c$ (N)	$F_d$ (N)	$3F_d$ (N)	$4F_d$ (N)	$5F_d$ (N)
TBA+ ( $\approx$ TPB $-$ )	$4.9 \times 10^{-10}$			$2.4 \times 10^{-10}$				
CB	$2.2 \times 10^{-10}$	1.55	$5.2 \times 10^{-30}$		$3.9 \times 10^{-11}$	$1.2 \times 10^{-10}$	$1.5 \times 10^{-10}$	$1.9 \times 10^{-10}$
o-DCB	$2.3 \times 10^{-10}$	2.25	$7.5 \times 10^{-30}$		$6.8 \times 10^{-11}$	$2.0 \times 10^{-10}$	$2.7 \times 10^{-10}$	$3.4 \times 10^{-10}$
DMSO	$2.2 \times 10^{-10}$	3.96	$1.3 \times 10^{-29}$		$2.5 \times 10^{-10}$	$7.5 \times 10^{-10}$	$1.0 \times 10^{-9}$	$1.3 \times 10^{-9}$

tor, as shown in Fig. 7(b). The dipole vector is assumed to be perpendicular to the conductor surface.  $l$  is the distance between  $+q$  and  $-q$ , and  $a$  is the distance between the conductor surface and the center of  $l$ . Thus,  $F_d$  is expressed as

$$F_d = \frac{q^2}{4\pi\epsilon_0} \left\{ \frac{1}{[2(a - \frac{l}{2})]^2} + \frac{1}{[2(a + \frac{l}{2})]^2} - \frac{1}{2a^2} \right\}. \quad (\text{A2})$$

The dipole moment  $\mu_d$  is defined as  $\mu_d = ql$ . By applying an infinitesimal separation to the two charges, i.e.,  $l \rightarrow 0$ , keeping the magnitude of  $\mu_d$ , the two-charge system can be treated as a point electric dipole. Thus, Eq. (A2) is written as

$$F_d = \frac{3\mu_d^2}{32\pi\epsilon_0 a^4} \quad (\text{A3})$$

by eliminating the terms of  $l^2$  in Eq. (A2).

The values of the image force calculated using Eq. (A1) for TBA+ ( $\approx$  TPB $-$ ) and using Eq. (A3) for CB, o-DCB, and DMSO are shown in Table I. For the volume of a solvent molecule, we referred to Ref. [53] for TBA+, Ref. [54] for CB and o-DCB, and Ref. [55] for DMSO, and calculated equivalent molecular radius assuming a sphere. Thus, a point dipole is placed at the center of the sphere. The distance between the electrode and the point dipole is assumed to be equal to the radius of the sphere, i.e.,  $a = r$ . The radii of CB, o-DCB, and DMSO are all smaller than half of the radius of TBA+. Considering their molecular sizes, a single TBA+ ion

needs to displace three to five solvent molecules to contact the electrode. Therefore,  $F_c$  should be compared to the sum of the image forces of the multiple molecules, not  $F_d$ . In this sense, the values of  $3F_d$ ,  $4F_d$ , and  $5F_d$  for CB, o-DCB, and DMSO are listed in Table I. As an example, when comparing the value of  $F_c$  with the values of  $4F_d$ , the attractive force from the electrode is TBA+  $>$  CB, TBA+  $\approx$  o-DCB, and TBA+  $<$  DMSO.

## APPENDIX B: SAMPLE PREPARATION AND MEASUREMENT CONDITION

Tetrabutylammonium tetraphenylborate (TBATPB: Aldrich purity  $>$  99%) was used as an electrolyte and added to several solvents at different concentrations. The electrolyte solution samples prepared are summarized in Table II. The solution was injected into a parallel-plate glass cell with indium tin oxide electrodes, the area and the distance between electrodes of which were  $1.13 \text{ cm}^2$  and  $22.6 \text{ }\mu\text{m}$ , respectively. The complex impedance of the cell was measured in the frequency range of 0.001 Hz and 10 KHz at  $20 \text{ }^\circ\text{C}$  using a Solartron 1260 frequency response analyzer connected to a 1296 dielectric interface. As can be seen from Eqs. (8)–(12), the complex dielectric constants brought about by SCP and DDL depend on the concentration of mobile ions, diffusion coefficient, and the distance between electrodes. On the other hand, the dielectric dispersion property of the SCP mode is different from that of the GC mode as shown in Fig. 2.

TABLE II. Electrolyte solution samples prepared for experiment.

Solvent	Dipole moment (D)	$\epsilon_{\text{sol}}$	TBATPB concentration		
			mol/L	$(\text{m}^{-3})$	
Bromobenzene (BB: Merck, purity $>$ 99%)	1.74	5.2	50 ppb	$1.3 \times 10^{-7}$	$8.0 \times 10^{19}$
			100 ppb	$2.6 \times 10^{-7}$	$1.6 \times 10^{20}$
			200 ppb	$5.2 \times 10^{-7}$	$3.2 \times 10^{20}$
			500 ppb	$1.3 \times 10^{-6}$	$8.0 \times 10^{20}$
Chlorobenzene (CB: Merck, purity $>$ 99%)	1.55	5.7	50 ppb	$9.9 \times 10^{-8}$	$5.9 \times 10^{19}$
			500 ppb	$9.9 \times 10^{-7}$	$5.9 \times 10^{20}$
			5 ppm	$9.9 \times 10^{-6}$	$5.9 \times 10^{21}$
			50 ppm	$9.9 \times 10^{-5}$	$5.9 \times 10^{22}$
1,2-Dichlorobenzene (o-DCB: Merck, purity $>$ 99%)	2.25	9.9	50 ppb	$1.2 \times 10^{-7}$	$7.0 \times 10^{19}$
			500 ppb	$1.2 \times 10^{-6}$	$7.0 \times 10^{20}$
			5 ppm	$1.2 \times 10^{-5}$	$7.0 \times 10^{21}$
			50 ppm	$1.2 \times 10^{-4}$	$7.0 \times 10^{22}$
Dimethylsulphoxide (DMSO: Aldrich, purity $>$ 99%)	3.96	47.2	500 ppm	$9.8 \times 10^{-4}$	$5.9 \times 10^{23}$

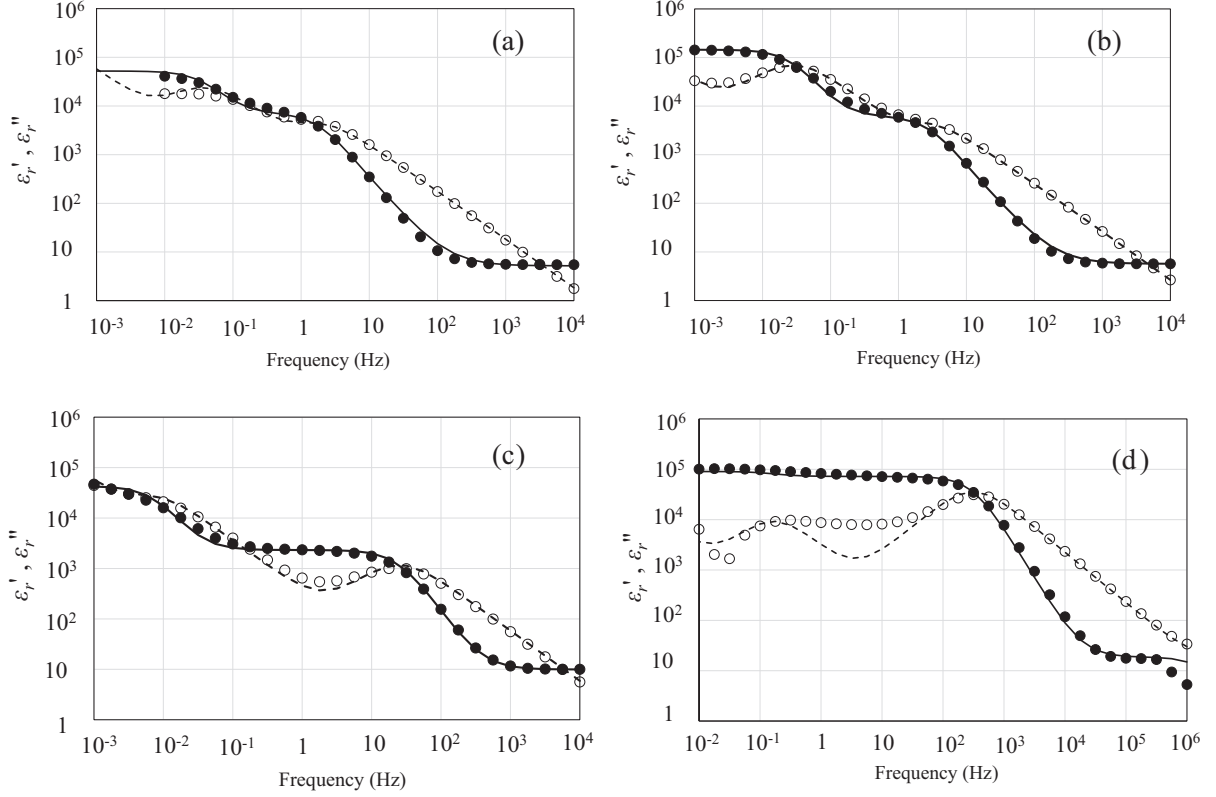


FIG. 8. Frequency dependences of complex dielectric constant for electrolytic solutions. (a) TBATPB 500 ppb in BB. (b) TBATPB 500 ppb in CB. (c) TBATPB 500 ppb in o-DCB. (d) TBATPB 500 ppm in DMSO. Filled and open circles represent observed values of  $\epsilon'_r$  and  $\epsilon''_r$ , respectively. Solid and dashed lines represent calculated values fitted to the observed values.

Therefore, the choice of frequency range and cell thickness is very important in the measurement. We determined the cell thickness and the frequency range so that the two dielectric dispersion properties could be clearly distinguished. The ac voltage applied to the cell was 0.005 V (rms), which satisfies the relationship that  $eV < kT$ . The complex impedance was then transformed to the complex dielectric constant  $\epsilon_r^* (= \epsilon'_r - i\epsilon''_r)$ .

### APPENDIX C: PHYSICAL PARAMETERS DETERMINED BY DATA ANALYSIS

The frequency dependences of  $\epsilon_r^*$  measured for the TBATPB solution samples described in Table II were analyzed by using the equivalent circuit given in Fig. 4. For all the samples, the measured values of  $\epsilon_r^*$  were well fitted by the calculated values. As an example, the analytical results for BB-TBATPB (500 ppb), CB-TBATPB (500 ppb),

TABLE III. Physical parameters determined by data analysis I.

Solvent	TBATPB concentration		$D$ ( $\text{m}^2/\text{s}$ )	$\mu$ ( $\text{m}^2/\text{Vs}$ )	$c_0$ ( $\text{m}^{-3}$ )	$C_m$ ( $\text{F}/\text{m}^2$ )	$R_m$ ( $\Omega/\text{m}^2$ )	
	(mol/L)	( $\text{m}^{-3}$ )						
BB	50 ppb	$1.3 \times 10^{-7}$	$8.0 \times 10^{19}$	$3.3 \times 10^{-10}$	$1.3 \times 10^{-8}$	$3.5 \times 10^{19}$	$3.0 \times 10^{-2}$	$6.0 \times 10^3$
	100 ppb	$2.6 \times 10^{-7}$	$1.6 \times 10^{20}$	$3.5 \times 10^{-10}$	$1.4 \times 10^{-8}$	$6.0 \times 10^{19}$	$5.0 \times 10^{-2}$	$4.0 \times 10^3$
	200 ppb	$5.2 \times 10^{-7}$	$3.2 \times 10^{20}$	$3.5 \times 10^{-10}$	$1.4 \times 10^{-8}$	$1.2 \times 10^{20}$	$5.0 \times 10^{-2}$	$7.0 \times 10^3$
	500 ppb	$1.3 \times 10^{-6}$	$8.0 \times 10^{20}$	$3.7 \times 10^{-10}$	$1.5 \times 10^{-8}$	$2.2 \times 10^{20}$	$5.0 \times 10^{-2}$	$3.0 \times 10^3$
CB	50 ppb	$9.9 \times 10^{-8}$	$5.9 \times 10^{19}$	$6.0 \times 10^{-10}$	$2.4 \times 10^{-8}$	$3.2 \times 10^{19}$	$1.3 \times 10^{-1}$	$6.0 \times 10^3$
	500 ppb	$9.9 \times 10^{-7}$	$5.9 \times 10^{20}$	$6.5 \times 10^{-10}$	$2.6 \times 10^{-8}$	$1.8 \times 10^{20}$	$1.3 \times 10^{-1}$	$6.0 \times 10^3$
	5 ppm	$9.9 \times 10^{-6}$	$5.9 \times 10^{21}$	$6.8 \times 10^{-10}$	$2.7 \times 10^{-8}$	$7.0 \times 10^{20}$	$1.3 \times 10^{-1}$	$2.0 \times 10^3$
	50 ppm	$9.9 \times 10^{-5}$	$5.9 \times 10^{22}$	$7.0 \times 10^{-10}$	$2.8 \times 10^{-8}$	$2.8 \times 10^{21}$	$1.3 \times 10^{-1}$	$2.0 \times 10^3$
o-DCB	50 ppb	$1.2 \times 10^{-7}$	$7.0 \times 10^{19}$	$4.0 \times 10^{-10}$	$1.6 \times 10^{-8}$	$6.5 \times 10^{19}$	$6.0 \times 10^{-2}$	$6.0 \times 10^3$
	500 ppb	$1.2 \times 10^{-6}$	$7.0 \times 10^{20}$	$4.2 \times 10^{-10}$	$1.7 \times 10^{-8}$	$6.2 \times 10^{20}$	$5.0 \times 10^{-2}$	$3.0 \times 10^3$
	5 ppm	$1.2 \times 10^{-5}$	$7.0 \times 10^{21}$	$4.0 \times 10^{-10}$	$1.6 \times 10^{-8}$	$6.0 \times 10^{21}$	$5.0 \times 10^{-2}$	$3.0 \times 10^3$
DMSO	50 ppm	$1.2 \times 10^{-4}$	$7.0 \times 10^{22}$	$4.0 \times 10^{-10}$	$1.6 \times 10^{-8}$	$4.0 \times 10^{22}$	$5.0 \times 10^{-2}$	$2.0 \times 10^3$
	500 ppm	$9.8 \times 10^{-4}$	$5.9 \times 10^{23}$	$2.7 \times 10^{-10}$	$1.1 \times 10^{-8}$	$5.9 \times 10^{23}$	$1.0 \times 10^{-1}$	$2.0 \times 10^3$



TABLE IV. Physical parameters determined by data analysis II.

Solvent	TBATPB concentration	$\epsilon_{\text{sol}}$	$v_{\text{av}}$ (m/s)	$\xi_a$ (m/s)	$\log(\xi_a)$	$\epsilon_{\text{eff}}$	$\epsilon_{\text{max}}$	$\epsilon_{\text{eff}}/\epsilon_{\text{max}}$	$\log(\epsilon_{\text{eff}}/\epsilon_{\text{max}})$
BB	50 ppb	5.2	$2.9 \times 10^{-6}$	$6.0 \times 10^{-6}$	-5.22	$1.51 \times 10^3$	$1.51 \times 10^3$	1.00	0.00
	100 ppb	5.2	$3.1 \times 10^{-6}$	$6.0 \times 10^{-6}$	-5.22	$2.58 \times 10^3$	$2.58 \times 10^3$	1.00	0.00
	200 ppb	5.2	$3.1 \times 10^{-6}$	$5.0 \times 10^{-6}$	-5.30	$5.15 \times 10^3$	$5.15 \times 10^3$	1.00	0.00
	500 ppb	5.2	$3.2 \times 10^{-6}$	$5.0 \times 10^{-6}$	-5.30	$9.44 \times 10^3$	$9.44 \times 10^3$	1.00	0.00
	50 ppm	5.7	$5.3 \times 10^{-6}$	$1.3 \times 10^{-5}$	-4.89	$1.47 \times 10^3$	$1.47 \times 10^3$	1.00	0.00
CB	500 ppb	5.7	$5.7 \times 10^{-6}$	$1.1 \times 10^{-5}$	-4.96	$8.22 \times 10^3$	$8.22 \times 10^3$	1.00	0.00
	5 ppm	5.7	$6.0 \times 10^{-6}$	$9.0 \times 10^{-6}$	-5.05	$2.50 \times 10^4$	$3.20 \times 10^4$	0.78	-0.11
	50 ppm	5.7	$6.1 \times 10^{-6}$	$4.0 \times 10^{-6}$	-5.40	$1.50 \times 10^4$	$1.28 \times 10^5$	0.12	-0.93
o-DCB	50 ppb	9.9	$3.5 \times 10^{-6}$	$1.4 \times 10^{-6}$	-5.85	70	$2.98 \times 10^3$	$2.35 \times 10^{-2}$	-1.63
	500 ppb	9.9	$3.7 \times 10^{-6}$	$2.5 \times 10^{-7}$	-6.60	55	$2.83 \times 10^4$	$1.94 \times 10^{-3}$	-2.71
	5 ppm	9.9	$3.5 \times 10^{-6}$	$1.2 \times 10^{-7}$	-6.92	90	$2.56 \times 10^5$	$3.52 \times 10^{-4}$	-3.45
DMSO	50 ppm	9.9	$3.5 \times 10^{-6}$	$8.0 \times 10^{-8}$	-7.10	300	$1.83 \times 10^6$	$1.64 \times 10^{-4}$	-3.78
	500 ppm	47.2	$2.4 \times 10^{-6}$	$5.0 \times 10^{-8}$	-7.30	1200	$2.69 \times 10^7$	$4.46 \times 10^{-5}$	-4.35

o-DCB-TBATPB (500 ppb), and DMSO-TBATPB (500 ppm) solutions are shown in Fig. 8. The physical parameters deter-

mined by curve fitting for all solution samples are summarized in Tables III and IV.

- [1] G. Jaffé, *Phys. Rev.* **85**, 354 (1952).  
[2] H. Chang and G. Jaffé, *J. Chem. Phys.* **20**, 1071 (1952).  
[3] J. R. Macdonald, *Phys. Rev.* **92**, 4 (1953).  
[4] R. Friauf, *J. Chem. Phys.* **22**, 1329 (1954).  
[5] P. W. M. Jacobs and J. N. Maycock, *J. Chem. Phys.* **39**, 757 (1963).  
[6] G. M. Anderson, *J. Chem. Phys.* **40**, 628 (1964).  
[7] B. J. H. Jackson and D. A. Young, *Trans. Faraday Soc.* **63**, 2246 (1967).  
[8] J. H. Beaumont and P. W. Jacobs, *J. Phys. Chem. Solids* **28**, 657 (1967).  
[9] C. G. J. Baker and E. R. Buckle, *Trans. Faraday Soc.* **64**, 469 (1968).  
[10] F. Stern and C. Weaber, *J. Phys. C* **3**, 1736 (1970).  
[11] R. Coelho, *Rev. Phys. Appl.* **18**, 137 (1983).  
[12] H. Schütt and E. Gerdes, *J. Non-Cryst. Solids* **144**, 1 (1992).  
[13] M. Z. Bazant, K. Thornton, and A. Ajdari, *Phys. Rev. E* **70**, 021506 (2004).  
[14] G. Barbero and A. Alexe-Ionescu, *Liq. Cryst.* **32**, 943 (2005).  
[15] A. D. Hollingsworth and D. A. Saville, *J. Colloid Interface Sci.* **257**, 65 (2003).  
[16] R. J. Klein, S. Zhang, S. Dou, B. H. Jones, R. H. Colby, and J. Runt, *J. Chem. Phys.* **124**, 144903 (2006).  
[17] R. J. Kortschot, A. P. Philipse, and B. H. Erné, *J. Phys. Chem. C* **118**, 11584 (2014).  
[18] F. R. G. B. Silva, R. Rossato, E. K. Lenzi, R. S. Zola, H. V. Ribeiro, M. K. Lenzi, and G. Gonçalves, *J. Electroanal. Chem.* **746**, 25 (2015).  
[19] I. Borukhov, D. Andelman, and H. Orland, *Phys. Rev. Lett.* **79**, 435 (1997).  
[20] M. S. Kilic, M. Z. Bazant, and A. Ajdari, *Phys. Rev. E* **75**, 021502 (2007).  
[21] A. Abrashkin, D. Andelman, and H. Orland, *Phys. Rev. Lett.* **99**, 077801 (2007).  
[22] D. Frydel, *J. Chem. Phys.* **134**, 234704 (2011).  
[23] D. Frydel and Y. Levin, *J. Chem. Phys.* **138**, 174901 (2013).  
[24] A. Levy, D. Andelman, and H. Orland, *J. Chem. Phys.* **139**, 164909 (2013).  
[25] A. Sawada, *J. Chem. Phys.* **126**, 224515 (2007).  
[26] A. Sawada, *Phys. Rev. E* **93**, 052608 (2016).  
[27] E. M. Purcell and D. J. Morin, *Electricity and Magnetism*, 3rd ed. (Cambridge University Press, New York, 2014), p. 500.  
[28] S. Uemura, *J. Polym. Sci., Polym. Phys. Ed.* **10**, 2155 (1972).  
[29] D. Frydel, *Adv. Chem. Phys.* **160**, 209 (2016).  
[30] A. Sawada, *J. Appl. Phys.* **100**, 074103 (2006).  
[31] J. R. Macdonald, *J. Chem. Phys.* **54**, 2026 (1971).  
[32] A. D. Hollingsworth, *Curr. Opin. Colloid Interface Sci.* **18**, 157 (2013).  
[33] C. Grosse and A. V. Delgado, *Curr. Opin. Colloid Interface Sci.* **18**, 161 (2013).  
[34] A. Sawada, K. Tarumi, and S. Naemura, *Jpn. J. Appl. Phys., Part 1* **38**, 1423 (1999).  
[35] H. Mada and A. Nishikawa, *Jpn. J. Appl. Phys.* **32**, L1009 (1993).  
[36] H. Naito, Y. Yokoyama, S. Murakami, M. Imai, M. Okada, and A. Sugimura, *Mol. Cryst. Liq. Cryst.* **262**, 249 (1995).  
[37] A. Sawada, Y. Nakazono, K. Tarumi, and S. Naemura, *Mol. Cryst. Liq. Cryst.* **318**, 225 (1998).  
[38] A. Sawada, K. Tarumi, and S. Naemura, *Jpn. J. Appl. Phys., Part 1* **38**, 1418 (1999).  
[39] M. Costa, R. Altafim, and A. Mammanna, *Liq. Cryst.* **28**, 1779 (2001).  
[40] F.-C. Lin, P.-C. Wu, B.-R. Jian, and W. Lee, *Adv. Condens. Mater. Phys.* **2013**, 271574 (2013).  
[41] R. Nasri, T. Missaoui, A. Hbib, and T. Soltani, *Liquid Crystals* **48**, 1429 (2021).  
[42] S. Uemura, *J. Polym. Sci., Polym. Phys. Ed.* **12**, 1177 (1974).  
[43] B. S. Krumgalz, *J. Chem. Soc., Faraday Trans. 1* **78**, 437 (1982).  
[44] B. S. Krumgalz, *J. Chem. Soc., Faraday Trans. 1* **79**, 571 (1983).

- [45] J. R. Smith, *Phys. Rev.* **181**, 522 (1969).
- [46] N. D. Lang and W. Kohn, *Phys. Rev. B* **1**, 4555 (1970).
- [47] A. Kiejna and K. F. Wojciechowski, *Metal Surface Electron Physics*, 1st ed. (Elsevier Science Japan, Tokyo, 1996).
- [48] S. Amokrane and J. P. Badiali, *J. Electroanal. Chem.* **266**, 21 (1989).
- [49] W. Schmickler, *Chem. Rev.* **96**, 3177 (1996).
- [50] D. Bérard, M. Kinoshita, X. Ye, and G. Patey, *J. Chem. Phys.* **101**, 6271 (1994).
- [51] M. Yamamoto, M. Kinoshita, and T. Kakiuchi, *Electrochim. Acta* **46**, 165 (2000).
- [52] According to the correlation between  $\xi_a$  and  $\varepsilon_{\text{eff}}/\varepsilon_{\text{max}}$  shown in Fig. 6,  $\varepsilon_{\text{eff}}$  should decrease with decreasing  $\xi_a$  in the range below  $10^{-5}$  m/s; nevertheless, this effect is not taken into account in this simulation of  $\varepsilon_r^*$ .
- [53] I. Larramendi, I. Lozano, M. Enterría, R. Cid, M. Echeverría, S. Peña, J. Carrasco, H. Manzano, G. Beobide, I. Landa-Medrano, T. Rojo, and N. Ortiz-Vitoriano, *Adv. Energy Mater.* **12**, 2102834 (2022).
- [54] M. Jurkiewicz and R. Pelech, *Int. J. Mol. Sci.* **22**, 13152 (2021).
- [55] M. Akkoyun, C. Carrot, and B. Blottière, *Appl. Rheol.* **24**, 13487 (2014).